Nuclear Inst. and Methods in Physics Research, A 898 (2018) 98–104

Contents lists available at ScienceDirect

Nuclear Inst. and Methods in Physics Research, A

journal homepage: www.elsevier.com/locate/nima

# A compact Time-Of-Flight detector for space applications: The LIDAL system

A. Rizzo [a,b,*], L. Narici [a,b], R. Messi [a,b], P. Cipollone [b], C. De Donato [b], L. Di Fino [a], M. Iannilli [a,b], C. La Tessa [d,c], C. Manea [c], G. Masciantonio [b], M.C. Morone [a,b], G. Nobili [b], D. Pecchi [a,b], P. Picozza [a,b], E. Reali [a,b], M. Rovituso [c], F. Tommasino [d,c], G. Vitali [a,b]

[a] University of Rome "Tor Vergata", Physics Department, via della Ricerca Scientifica 1, 00100 Rome, Italy
[b] INFN Sezione Roma Tor Vergata, via della Ricerca Scientifica 1, 00100 Rome, Italy
[c] Trento Institute for Fundamental Physics and Application - TIFPA INFN -Via Sommarive 14, 38123 Povo (Trento), Italy
[d] University of Trento, Physics Department, via Sommarive 14, 38123 Povo (Trento), Italy

ARTICLE INFO

*Keywords:*
Charged particle detector
TOF
Time-Of-Flight
Time resolution
Space
International space station
Scintillators

ABSTRACT

LIDAL (Light Ion Detector for ALTEA system) is a compact detector designed to upgrade ALTEA (Anomalous Long Term Effects on Astronauts) silicon detector apparatus, in order to study in detail the low-Z part of ions spectrum inside the International Space Station (ISS) and to enhance the Particle Identification (PID) capability of the system.

The new detector is designed to trigger ALTEA and to perform Time-Of-Flight measurements. It is based on plastic scintillators for fast timing applications read by Photo-Multiplier-Tubes (PMTs). A custom Front End Electronics (FEE) has been designed to reach time resolutions less than 100 ps ($\sigma$) for protons.

A LIDAL prototype has been developed at the University of Rome Tor Vergata to test the timing performance of the scintillators, the PMTs and of the custom FEE using the proton beam line at the TIFPA (Trento Institute for Fundamentals Physics Applications) center in Trento, Italy. The results of these tests are reported and discussed. They have also been used for a preliminary evaluation of the Particle Identification (PID) capability of the final LIDAL-ALTEA detector system in response to the ions spectra expected on-board the ISS.

## 1. Introduction

Very fast plastic scintillator detectors represent nowadays a well established technology to be used for Time-Of-Flight (TOF) measurements, allowing to design compact devices suitable for space applications.

The LIDAL detector (Light Ion Detector for ALTEA) exploits this technology for radiation monitoring in human space habitats. It extends the sensitivity of the ALTEA apparatus (Anomalous Long Term Effects on Astronauts) to the low-Z ions since it allows to lower the trigger energy thresholds and to enhance the PID capability thanks to TOF measurements. The detector is based on fast plastic scintillators read by Photo-Multiplier-Tubes (PMTs); a custom fast Front-End-Electronics (FEE) allows LIDAL to reach time resolutions ($\sigma$) below 100 ps for proton energies expected onboard the International Space Station (ISS).

ALTEA apparatus has already been hosted onboard the International Space Station (ISS) (2006–2012) in missions aiming at the study of the ISS radiation environment [1–3]. The integration between the two detectors is shown in Fig. 1, where three ALTEA silicon telescopes (hereafter SDUs, Silicon Detector Units) are placed between the two LIDAL Detector Units (hereafter LDU). The possibility to have an efficient PID by matching the velocity $\beta$ measured by LIDAL with the deposited energy measured by ALTEA for each event, will allow for the first time to measure in real time the ratio $Z^2/\beta^2$, a fundamental parameter related to the radiation risk for astronauts [4].

A first LIDAL prototype with two fast scintillator bars has been designed and constructed at the University of Rome Tor Vergata (URTV), featuring a custom fast FEE, based on the NINO chip (a fast discriminator and shaper [5]). The FEE output is processed by a CAEN V1290 Time to Digital Converter (TDC) module, including the CERN HpTDC chip, used in high resolution mode (32bit/channel). This chip will be used in the Data Acquisition (DAQ) electronics designed for the final LIDAL-ALTEA apparatus. Tests of the prototype have been performed at the Trento Institute for Fundamentals Physics Applications (TIFPA) proton beam line in Trento (Italy) to demonstrate that a time resolution better

* Corresponding author at: University of Rome "Tor Vergata", Physics Department, via della Ricerca Scientifica 1, 00100 Rome, Italy.
*E-mail address:* alessandro.rizzo@roma2.infn.it (A. Rizzo).

https://doi.org/10.1016/j.nima.2018.05.009
Received 13 November 2017; Received in revised form 23 March 2018; Accepted 4 May 2018
Available online 18 May 2018

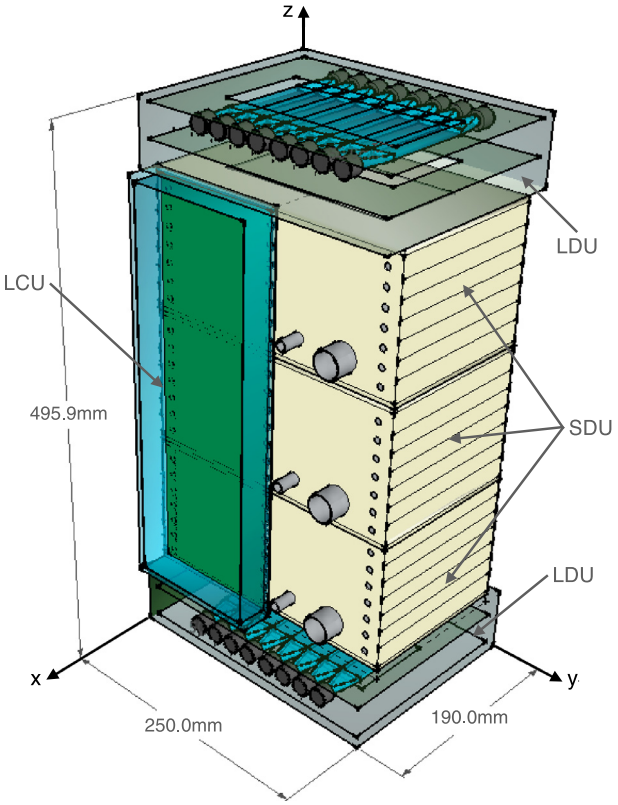


**Fig. 1.** Sketch of the LIDAL-ALTEA system in the final configuration designed to fly onboard the ISS (namely Flight Model or FM). The LIDAL detector will consist of three modules: two LDUs, each made of eight scintillators, and one LCU (LIDAL Collector Unit), for data acquisition. In between the two LDU modules three ALTEA SDUs are placed . Each ALTEA SDU is a particle telescope with six stripped silicon planes (380 μm thick, $8 \times 16$ cm$^2$ active area) stacked in a tower configuration, able to measure the energy loss and to reconstruct the track of a particle passing through. The Energy loss measured by ALTEA SDUs and the velocity measured by LIDAL will allow an efficient PID for a reliable risk assessment in real time.

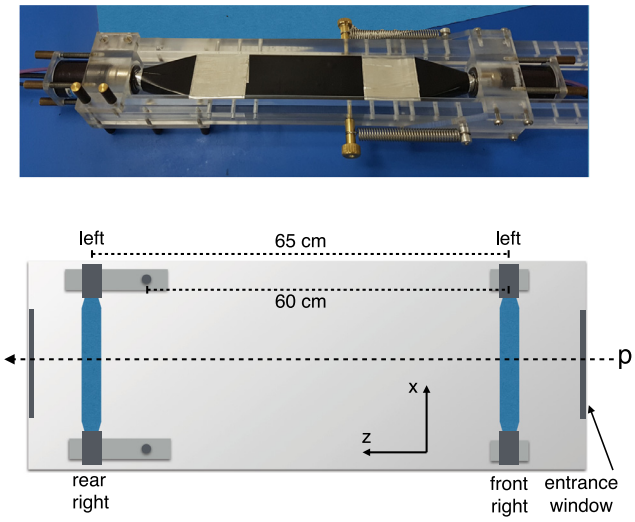


**Fig. 2.** *top*: A LIDAL scintillation unit, consisting in a scintillator bar coupled with two PMMA light guides and two PMTs, is shown. The traction springs of the plastic holder assure a constant and homogeneous pressure for the optical contacts between the different surfaces, obtained by a thin layer of optical grease. *bottom*: Two LIDAL scintillation units are placed at a distance $d$ which can be set at 60 or 65 cm inside the aluminum box. Hereafter the first scintillator facing the beam is the *front scintillator*, the other is the *rear scintillator*.

than 100 ps may be achieved by LIDAL for protons. The experimental apparatus, the results and the future perspectives are discussed in the following sections.

## 2. LIDAL prototype

The LIDAL prototype has been designed and constructed to test the characteristics of the detector and the related electronics using a particle beam, so its geometry is quite different from the final LIDAL-ALTEA system. For this reason some mechanical solutions used for this prototype will not be implemented in the final design of the apparatus to fly onboard the ISS.

The prototype has been developed using plastic scintillators EJ-230 (Eljen Technologies) for fast timing application [6] and HAMAMATSU Photo Multiplier Tubes (PMTs) RS9880-U210. The PMTs have a Quantum Efficiency (QE) of 40% in the wavelength spectrum emitted by the scintillator (between 375 and 400 nm), a nominal rise time of 570 ps and compact dimensions [7]. The plastic scintillator EJ-230 is characterized by a rise time of 500 ps and a light output of 9700 photons for 1 MeV deposited electron energy [6]. These characteristics assure the fast timing response required to perform the TOF measurements together with a light output sufficient to provide a good trigger signal. The final scintillator dimensions ($90 \times 25 \times 8$ mm$^3$) have been chosen to maximize the timing resolution, according to FLUKA simulation results [8,9]. Both extremities of the scintillator bars are coupled to PMMA light guides, specifically designed to maximize the light collected to the PMTs. The optical contacts with light guides and PMTs are realized using high quality optical grease (BC630). A scintillation unit, formed by a scintillator bar, two PMMA light guides and two PMTs, is assembled using a plastic holder shown at the top of Fig. 2 . Two traction springs at both sides of the plastic holder assure a constant and homogeneous pressure among the optical contact surfaces. To maximize the light collected at the extremities, scintillator bars and light guides are wrapped in mylar foil, while multiple layers of black tape assure that the detector is light-tightened. Two scintillation units have been placed inside an aluminum box at a distance that can be set at 60 or 65 cm (see Fig. 2, bottom). The entrance window of the box is closed by a double wrap of black tape to light-tight the system.

The PMT signal is discriminated and shaped by the NINO chip in the FEE and then sent to the CAEN V1290 module. The module is based on the CERN HpTDC chip, which is used in high resolution mode (32bit/channel) to achieve the best timing resolution performance. A second and independent data acquisition chain has been set up to evaluate the deposited energy in the scintillator bars: the split PMTs signals are sent to a low-threshold discriminator (CAEN 417) followed by a CAEN V792 QDC module. Ad-hoc electronic boards, which integrate the HpTDC and NINO chips, are currently being designed for the final LIDAL-ALTEA apparatus.

## 3. Test at TIFPA proton beam line

The detector prototype has been tested at the TIFPA proton beam line (Trento, Italy) to study the timing performance of the system including its custom FEE. Protons are delivered at the facility by a superconducting cyclotron with an energy which can be set at values ranging from 90 to 228 MeV, with a rate up to $10^9$ particles per second. The beam spot presents a round shape at the isocenter, with a diameter of about 15 mm. Several proton beam energies have been used in the tests at rates below 10 kHz. The low rate condition is achieved by putting in *dark current* mode the proton source inside the cyclotron. The high voltage of the source is set below the threshold used for the standard operations, resulting in low proton fluxes accelerated by the cyclotron. The monitoring devices along the beam line are not efficient at this

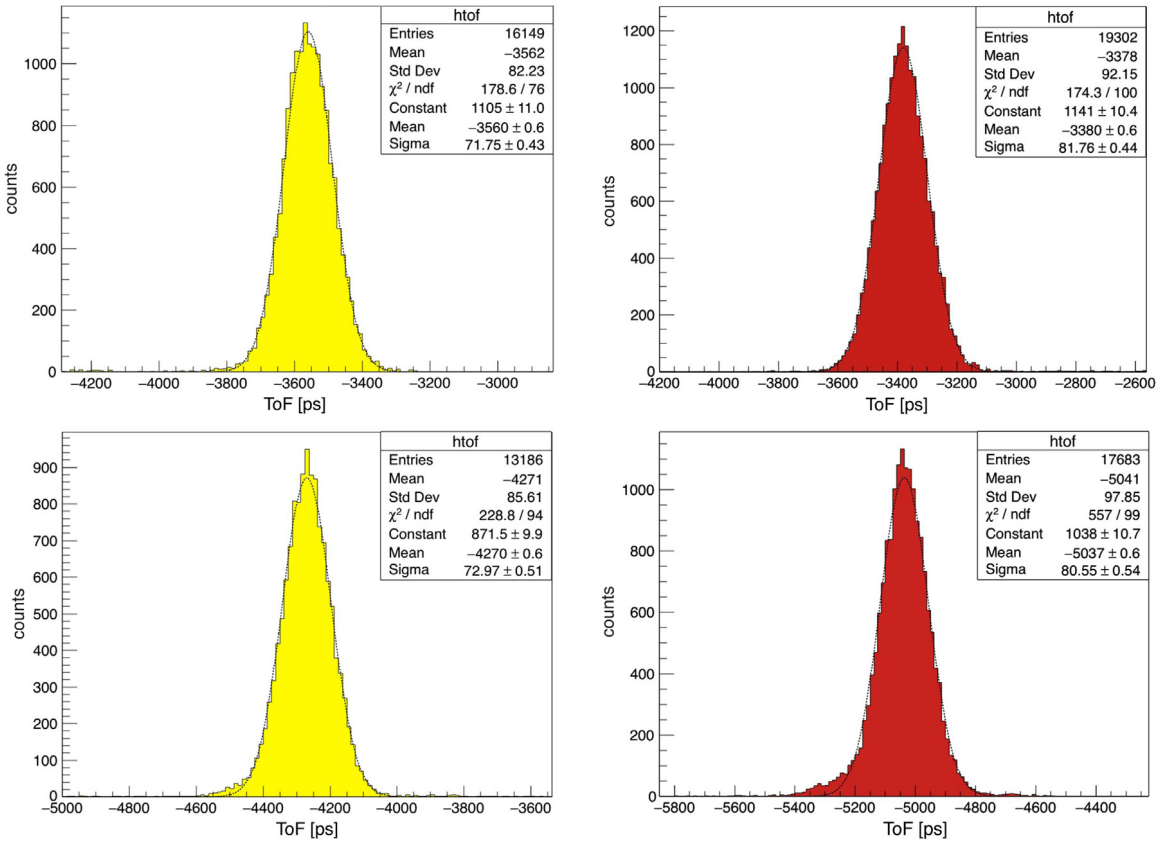


**Fig. 3.** Example of Time-Of-Flight distributions (color on-line) obtained setting a distance of 65 and 60 cm between the two scintillators. Top-Left: TOF distribution for 228 MeV protons obtained with scintillators placed at 65 cm. Top-Right: TOF distribution for 228 MeV protons obtained with scintillators placed at 60 cm. Bottom-Left: TOF distribution for 159 MeV protons obtained with scintillators placed at 65 cm. Bottom-Right: TOF distribution for 100 MeV protons obtained with scintillators placed at 60 cm. The Time-Of-Flight is calculated as the time difference between the left–right averaged times measured by rear and front scintillators.

low rates, resulting in larger beam energy and rate fluctuations [10]. As mentioned, the main goal of this measurement campaign is the evaluation of the timing resolution for protons at different energies. A study of the timing resolution of the system as a function of the impinging point of the incident particles has been also performed.

### 3.1. Time resolution

To measure the time resolution of the system, the DAQ is set in the auto-trigger configuration: an AND condition between front and rear scintillators is used to detect a crossing particle event. Passive delays due to coaxial cables have been equalized and the bias voltages have been carefully set for each PMT to match the gain values. Data have been acquired at five beam energies for the 65 cm baseline configuration (100, 131, 159, 193 and 228 MeV) and at three energies for the 60 cm baseline configuration (100, 159 and 228 MeV) while the beam impinged in the center of the scintillator bars. The Time-Of-Flight has been evaluated according to the following formula

$$TOF = \langle t_r \rangle - \langle t_f \rangle \tag{1}$$

where $\langle t_r \rangle$ and $\langle t_f \rangle$ are the average values of the times registered by the left ($t_i^L$) and the right ($t_i^R$) PMTs for rear (r) and front (f) scintillators, respectively:

$$\langle t_i \rangle = \frac{t_i^L + t_i^R}{2} \qquad i = r, f \tag{2}$$

It is possible to demonstrate that the TOF value defined according to the previous equation is independent from the speed of light inside the scintillator and from the scintillator length. An example of typical TOF measurements is given in Fig. 3.

**Table 1**
Summary of time resolution evaluated as the standard deviation of the time distribution in ps for the two baselines of 65 and 60 cm length.

| | 100 MeV | 131 MeV | 159 MeV | 193 MeV | 228 MeV |
|---|---|---|---|---|---|
| 65 cm | $\sigma = 73$ ps | $\sigma = 70$ ps | $\sigma = 73$ ps | $\sigma = 72$ ps | $\sigma = 75$ ps |
| 60 cm | $\sigma = 81$ ps | – | $\sigma = 70$ ps | – | $\sigma = 82$ ps |

The non-gaussian tails of the distributions in Fig. 3 are due to multiple light reflections inside the scintillator bar and in the light guides: the longest light path due to multiple reflections, results in a late-coming signal which falls far from the mean value. The tails are higher for lower kinetic energies because the spread on the beam spot size due to the straggling through the crossed materials is larger. This spread effect can result in particles hitting far from the central point of the scintillator, which can produce multiple reflections of scintillation light.

The time resolution has been evaluated as the standard deviation $\sigma$ of the Gaussian function used to fit the time distributions. No cuts on the deposited energy in the scintillator bars (QDC values) have been used in this part of the analysis (conservative approach). The results are summarized in Table 1 below.

The time resolution of the system has been also evaluated varying the impinging point of the beam on the detector, to study how the light reflections inside the scintillator bars affect the time duration of the signal. For the 65 cm long baseline configuration, three impinging points for 228 MeV proton beam energy have been used at 10, 20 and 30 mm from the center of the scintillator. Table 2 summarizes the obtained results.

The worst time resolution is expected in the proximity of the scintillator edges, due to the multiple reflections of the scintillation light

**Table 2**
Summary of time resolutions evaluated as the standard deviation of the time distribution in ps for different impinging point of the beam (228 MeV). The detector baseline is 65 cm long.

| Position | 0 (center) | +10 mm | +20 mm | +30 mm |
|---|---|---|---|---|
| $\sigma$ | 75 ps | 75 ps | 79 ps | 80 ps |

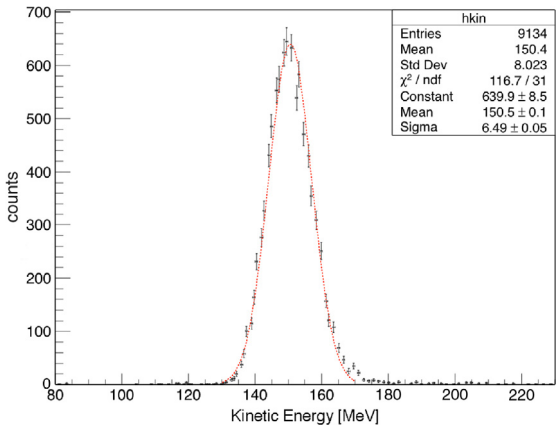


**Fig. 4.** The measured kinetic energy distribution for 159 MeV protons. The nominal energy of incoming protons is degraded by the first LIDAL scintillator itself plus a small scintillator placed upward, used to monitor the rate stability of the beam. The degraded energy has been evaluated to be 153 MeV (see text).

inside the bars that broaden the PMT signals. The results reported in Table 2 show this behavior. The small difference (5 ps) between the resolution values at the center and at 30 mm far from the center, shows how the small dimensions of the LIDAL scintillator bars helps in keeping this phenomenon under control. The obtained values fulfill the timing resolution constraint requested for LIDAL to remain lower than 100 ps.

### 3.2. Kinetic energy measurement and tracking capability

The kinetic energy and the beam profile have been reconstructed in the configuration with 60 cm long baseline to evaluate other detector performance. Three runs with beam impinging on the center of the scintillators (nominal energies 100, 159 and 228 MeV) have been acquired. Fig. 4 shows the measured kinetic energy ($T$) of the incoming protons ( for the 159 MeV beam), evaluated according to the formula (3)

$$T = \sqrt{\frac{m^2c^4}{1-\frac{\Delta^2}{c^2(TOF)^2}}} - mc^2 \tag{3}$$

where $m$ is the proton mass, $c$ the speed of light, $\Delta$ is the distance between scintillators.

The distribution has been fitted with a Gaussian function: in this specific case the mean kinetic energy results equal to $151 \pm 7$ MeV. This value must be compared with the degraded energy due to the interaction of the beam with the interposed material. During these runs, a small plastic scintillator (5 mm thick) placed before LIDAL detector was used to monitor the rate stability of the beam. This material budget should be added to the thickness of the LIDAL front scintillator. Using calculations made with $LISE^{++}$ software [11], the degraded kinetic energy of the particles is 153 MeV.

The convolution between the detector resolution and the beam energy spread provides the width of the distribution and can be considered the upper limit of the detector energy resolution, conservatively taken equal to the measures uncertainty.

The isocenter of the beam spot corresponds to the detector center for both scintillators. The nominal dimension of the beam at the isocenter is 12 mm (standard deviation) for the considered energy range. The dimension of the beam has been reconstructed by measuring the impinging point of the particles in each scintillator from the left–right arrival time difference recorded by the system. Fig. 5 shows the beam profile along the x axis (see Fig. 2) for 228 MeV protons.

**Table 3**
Summary of the kinetic energy and beam spot dimension measurements.

| Measurement | I | II | III |
|---|---|---|---|
| $T_{nominal}$ [MeV] | 100 | 159 | 228 |
| $T_{degraded}$ [MeV] | 85 | 153 | 226 |
| $T_{meas}$ [MeV] | $84 \pm 3$ | $151 \pm 7$ | $225 \pm 10$ |
| beam spot dimension front [mm] | 21 | 17 | 14 |
| beam spot dimension rear [mm] | 30 | 18 | 15 |

Table 3 summarizes the results.

As can be seen from the results shown in Fig. 5 and in Table 3, the dimension of the spot appears to be larger on the rear of the scintillator, because of the protons interaction with the front scintillator. The larger spot in the rear scintillator due to the degrading effect of the first scintillator on the beam, is clearly visible also by correlating the charge-to-digital (QDC) values measured for each event. Considering an exponential attenuation for the light inside the scintillators, we can define the following variables:

$$E_{front} = \sqrt{Q_L^F Q_R^F} \quad E_{rear} = \sqrt{Q_L^R Q_R^R} \tag{4}$$

where $Q_L^F$, $Q_R^F$ and $Q_L^R$ , $Q_R^R$ are the QDC channels acquired from the Left (L)/Right (R) PMTs of the front (F) and rear(R) scintillators, respectively. The correlation plot in Fig. 6 confirms that the energy released in the second scintillator is higher than the energy released in the first one. The QDC DAQ chain is completely independent from the TDC DAQ chain: it has been set up only to evaluate the quantity of light collected to the PMTs in order to design comparator circuits to drive the ALTEA trigger by LIDAL detector.

## 4. TOF contribution to the active detectors PID capability in space: a preliminary study

Particle identification plays a fundamental role in radiation risk assessment in space, because different health risks are related to different ions and their ionizing powers. Active detectors are largely used in human space habitat (e.g. DOSTEL [12], ALTEINO [13], Liulin-5 [14], RAD [15]) to measure the radiation field characterized by large dynamics in terms of time and kinetic energy. The PID with this kind of detectors is often done statistically, based on fits of the deposited energy spectrum acquired.

A preliminary study has been carried out to evaluate the contribution to the PID given by the TOF measurements performed by LIDAL to the ALTEA detector. In particular, the results obtained at the proton beam line for the LIDAL prototype have been projected to the case of the radiation field expected onboard the ISS. In this evaluation we considered one ALTEA SDU placed in between two LIDAL scintillator bars spaced by 60 cm and assumed a time resolution of 85 ps.

Kinetic energies and relative abundances of ions ranging from $Z = 1$ to $Z = 26$ inside the ISS have been generated according to the simulated spectra obtained using CREME96, which have already been used to characterize the spectrum detected by ALTEA [12,16] during the flight onboard the ISS. The signal in ALTEA SDU has been evaluated as follows: the deposited energy in 2 mm of silicon (equal to the total thickness of the six silicon planes inside the SDU) has been evaluated for each incoming ion, according to the Bethe–Bloch formula, with the density correction calculated according to [17]. The calculated deposited energy value has been smeared according to a Gaussian function, whose width, due to the straggling effect, was calculated according to [18]. The non-normal tracks have been also considered in this study, in terms of different thickness of silicon crossed by the particles as a function of the

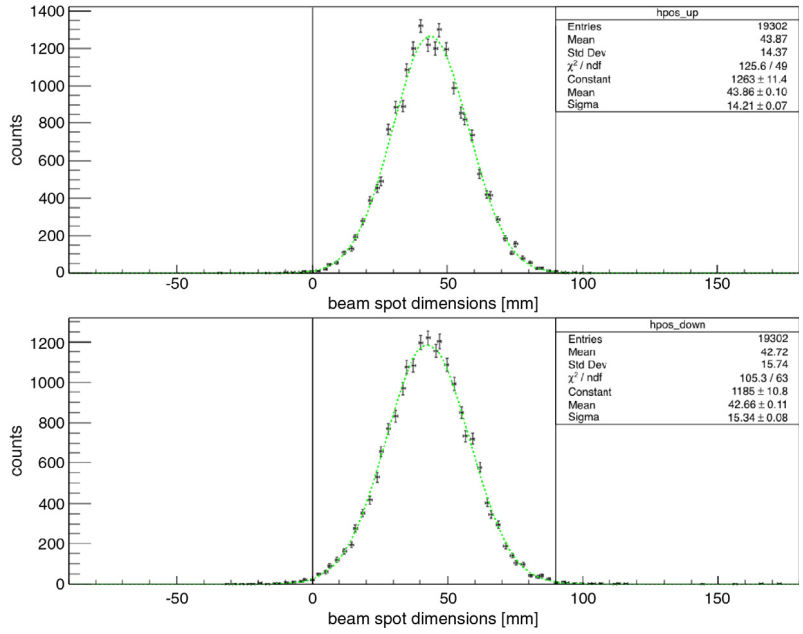


**Fig. 5.** Particle hit coordinate position along x axes measured by front and rear scintillators (see Fig. 2) . The black vertical lines indicate the physical dimension of the two scintillator bars.

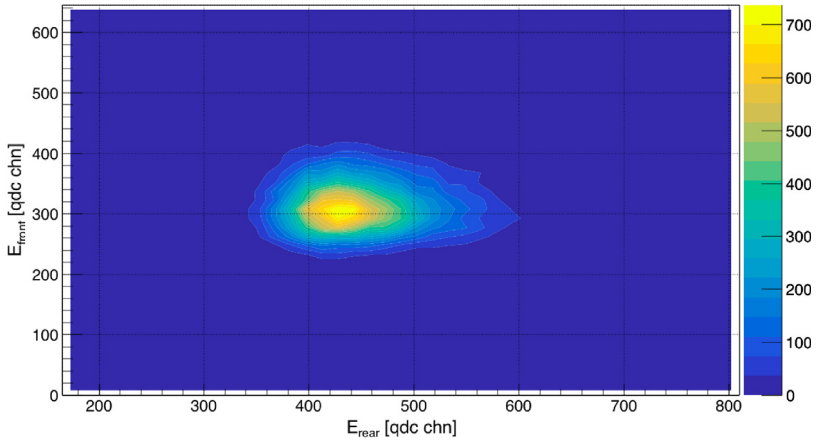


**Fig. 6.** Correlation between the QDC signals from the front and rear scintillators.

track angle, which can range between 0 (normal trajectory) to 0.186 rad. For each ion the trajectory angle has been generated according to a uniform distribution (isotropic source around the ISS) between the two limit values. The obtained result, considering also the acceptance energy windows of ALTEA SDU [1], is shown in Fig. 7.

As benchmark to compare the TOF contribution given by LIDAL to the PID capability of the system, three peaks are considered in particular: Boron, Carbon and Nitrogen. As shown in Fig. 7 the large overlapping of the peaks and their shape, which depends on several parameters (for example the amount of materials surrounding the detector as cables, rack and electronics passed by ions), gives large uncertainties in fit results.

To evaluate the TOF contribution given by LIDAL to the PID capability of ALTEA, TOF values of the considered events have been evaluated as follows. Starting from the ion kinetic energy value, the TOF value has been calculated considering a distance between the scintillators of 60 cm. The obtained value has been then smeared according to a Gaussian function with a $\sigma$ equal to the timing resolutions of 85 ps (value that include also the uncertainty for non-normal tracks). The result, merged with the energy deposited in ALTEA SDU, is shown in the two dimensional plot in Fig. 8

The projection on the y axis of the bi-dimensional plot corresponds to the histogram shown in Fig. 7, where neighboring ion peaks are largely overlapping. The information given by the velocity measured by LIDAL, resulting in the second dimension (x-axis) of the plot in Fig. 8, allows to disentangle the overlaying contributions. At a fixed value of $\gamma\beta$ measured by LIDAL, it correspond a slice on x axis of the bi-dimensional plot, where the neighboring peaks are much better separated.

An evaluation of the mean PID discrimination capability overall the whole $\gamma\beta$ range, can be done considering the events falling in between the two dotted lines in the bi-dimensional plot, that represents Bethe–Bloch formulas for carbon ions set at $Z = 12 \pm 0.5$. For $n = 92650$ detected carbon events, 1104 are miss-recognized as nitrogen, 1572 as boron and the corresponding estimated discrimination efficiency is equal to $\eta = 0.969 \pm 0.001$. The error has been evaluated as the standard deviation of the binomial distribution for the efficiency, equal to $\sigma = \sqrt{(\eta(1-\eta)/n)}$.

This preliminary study suggests that the LIDAL-ALTEA system will provide enhanced PID capability with respect to the ALTEA detector alone. Moreover, considering the small number of mis-recognized events for neighboring Boron, Carbon and Nitrogen ions, a real time PID seems feasible with a small uncertainty never reached before, opening the way

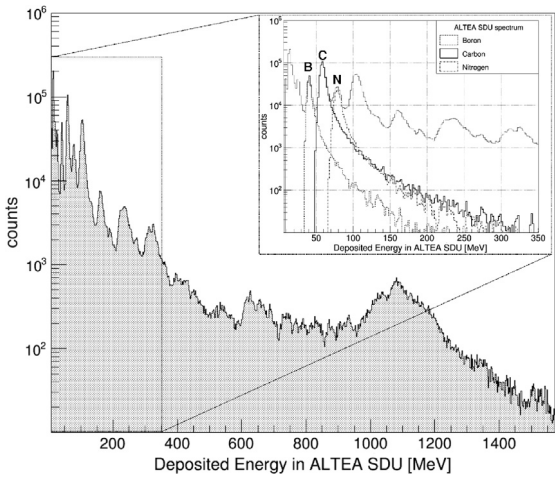


**Fig. 7.** Deposited energy spectrum in one ALTEA SDU placed between two LIDAL scintillators in about 20 days of data taking. The box presents an enlarged region of interest including Boron, Carbon and Nitrogen overlapping peaks.

to a more detailed and reliable real time risk assessment for astronauts for next space missions.

## 5. Conclusions and future perspectives

Tests at TIFPA proton beam line have shown that time resolution values well below the design goal of 100 ps have been achieved for the first LIDAL prototype. The chosen scintillators, the PMTs and the electronics have been tested showing performance better than the expected ones, confirming their useful implementation in the final LIDAL-ALTEA apparatus. For the LIDAL-ALTEA Flight Model, scintillators dimensions can be further reduced, in particular the thickness (from 8 mm to 4 mm), still assuring enough light output to trigger the system. This solution will contribute to enhance timing performance of the system, lowering the light path due to multiple internal light reflections. The technological solutions tested in this measurement campaign have shown that TOF measurements with a good time resolution are feasible also with a detector of compact dimensions.

The LIDAL-ALTEA system, which will be ready in august 2018, is manifested to be sent onboard the ISS in 2019. It will allow to characterize in detail and in real time the radiation environment inside a human space habitat, being sensitive to the whole ion spectra (Z = 1-26) and featuring enhanced PID capability. The ability of measuring parameters such as $Z^2/\beta^2$ individually for each particle using the independent information coming from the ToF measurements, provides an unprecedented tool for risk assessment for astronauts.

## Acknowledgment

The Financial contribution of ASI (Light Ions Detector for ALTEA (LIDAL) contract N. 2016-2-U.0) is acknowledged.

## References

[1] V. Zaconte, et al., ALTEA: the instrument calibration, Nucl. Instrum. Methods Phys. Res. 266 (2008) 2070–2078. http://dx.doi.org/10.1016/j.nimb.2008.02.072.
[2] L. Narici, et al., Heavy ions light flashes and brain functions: recent observations at accelerators and in spaceflight, New J. Phys. 10 (2008). http://dx.doi.org/10.1088/1367-2630/10/7/075010.
[3] V. Zaconte, et al., High energy radiation fluences in the ISS-USLab: ion discrimination and particle abundances, Radiat. Meas. 45 (2010). http://dx.doi.org/10.1016/j.radmeas.2012.07.006.
[4] F. Cucinotta, Space radiation cancer risk projections and uncertainties 2012, NASA TP 217375 (2013) 118–121.
[5] F. Aghinolfi, et al., NINO: an ultrafast low-power front-end amplifier discriminator for the time-of-flight detector in the ALICE experiment, IEEE Trans. Nucl. Sci. 51 (2004) 1974–1978. http://dx.doi.org/10.1109/TNS.2004.836048.
[6] Fast timing EJ-228, EJ-230. Available at: http://www.eljentechnology.com/products/plastic-scintillators/ej-228-ej-230. (Accessed October 2017).
[7] Hamamatsu R9880U PMT series. Available at: http://www.hamamatsu.com/resources/pdf/etd/R9880U_TPMH1321E.pdf. (Accessed October 2017).
[8] G. Battistoni, et al., The FLUKA code: Description and benchmarking, AIP Conf. Proc. 896 (2007) 31–49.
[9] A. Ferrari, et al., FLUKA: a multi-particle transport code, no. 004.4:539.1, CERN-2005-010; INFN-TC-2005-11; SLAC-R-77, 2005.
[10] F. Tommasino, et al., Proton beam characterization in the experimental room of the trento proton therapy facility, Nucl. Instrum. Methods Phys. Res. 869 (2017) 15–20. http://dx.doi.org/10.1016/j.nima.2017.06.017.
[11] O.B. Tarasov, D. Bazin, LISE + +: design your own spectrometer, Nucl. Phys. A 746 (2004) 411c–414c. http://dx.doi.org/10.1016/j.nuclphysa.2004.09.063.
[12] L. Narici, et al., Exploiting different active silicon detectors in the International Space Station: ALTEA and DOSTEL galactic cosmic radiation (GCR) measurements, J. Space Weather Space Climate A18 (2017). http://dx.doi.org/10.1051/swsc/2017016.
[13] M. Casolino, et al., The Sileye Alteino experiment on board the International Space Station, Nuclear Phys. B Proc. Suppl. 113 (2002) 71–78.

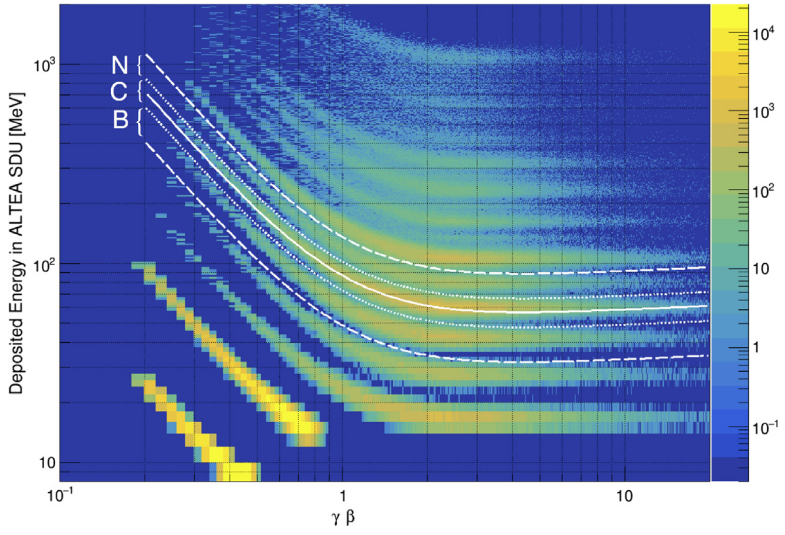


**Fig. 8.** Simulated spectrum acquired by LIDAL-ALTEA system in about 20 days of data taking on-board the ISS.

[14] J. Semkova, et al., Instrumentation for investigation of the depth-dose distribution by the Liulin 5 instrument of a human phantom on the Russian segment of ISS for estimation of the radiation risk during long term space flights, Adv. Space Res. 34 (2004) 1297–1301.
[15] Results from the iss-rad charged particle detector and comparison to msl-rad. Available at: http://wrmiss.org/workshops/twentysecond/Zeitlin.pdf. (Accessed March 2018).
[16] L. Narici, et al., Iron flux inside the International Space Station is measured to be lower than predicted, Radiat. Meas. 47 (2012) 1030–1034. http://dx.doi.org/10.1016/j.radmeas.2012.07.006.
[17] R.M. Sternheimer, et al., Density effect for the ionization loss of charged particles in various substances, At. Data Nucl. Data Tables 30 (1984) 261–271.
[18] C. Amsler, et al., Particle data group, Phys. Lett. B 67 (2008) 1030–1034.